FCP Report No. 20

FRACTURE FEATURE ANISOTROPY IN A MARTENSITIC STEEL PLATE

by

Richard H. Sailors
Formerly, Department of Theoretical and Applied Mechanics,
University of Illinois at Urbana-Champaign
Presently, Bucyrus-Erie Company, South Milwaukee, Wisconsin

ABSTRACT

The three mutually perpendicular fracture plane orientations in a martensitic steel plate were examined both metallographically and fractographically. The non-uniform distribution of inclusions and anisotropy in inclusion shape produced different appearing fractures, yet all were microscopically ductile. Detailed examination of fracture surfaces and fracture surface profiles illustrated the extent of void growth from sulfide inclusions before macroscopic fracture. This investigation emphasized the compatibility of conventional metallography and stereofractography in analyzing the fracture process.

A Report of the
FRACTURE CONTROL PROGRAM

College of Engineering, University of Illinois
Urbana, Illinois 61801
October, 1975

ACKNOWLEDGMENTS

This investigation was performed in the H. F. Moore Fracture Research Laboratory, Department of Theoretical and Applied Mechanics, University of Illinois at Urbana-Champaign, Illinois with support from the Fracture Control Program, College of Engineering, and the Advanced Research Project Agency, Department of Defense, under U. S. Department of the Army No. DAHC 17-72-6-7, ARPA Order No. 2169.

The author is also indebted to Professors H. T. Corten, J. Morrow, and G. M. Sinclair for valuable discussions and constant encouragement throughout his tenure at the University of Illinois. Thanks to Mrs. Darlene Mathine for typing the manuscript.

INTRODUCTION

The observation of second phase particles such as strengthening precipitates and non-metallic inclusions on the fracture surface of steel specimens clearly indicates their importance in the overall ductile fracture process. Although voids can be initiated by dislocation or vacancy mechanisms (1), second phase particles are the primary void initiators in practical engineering materials. Reductions in volume fraction of second phase particles, which can give smaller particles with no change in spacing or an increase in spacing with no change in size, or both simultaneously, have been shown in general to increase such things as fracture toughness, K_{Ic}, and true fracture strain, ϵ_f, (2, 3, 4). However, in wrought steels certain mechanical properties are very sensitive to shape and distribution of inclusions for a given volume fraction. For instance, fracture toughness, K_{Ic}, is the largest when the crack plane normal is in the longitudinal or primary rolling direction (RW or RT orientation), intermediate when it is in the transverse direction (WR or WT orientation), and smallest when it is in the short transverse or thickness direction (TR or TW orientation). The anisotropy in fracture toughness is large enough that, for instance in cylindrical pressure vessels, the steel plate's longitudinal direction is oriented to support the larger hoop compared to the axial stress. Anisotropy decreases as cleanliness increases and thus provides an additional advantage to increased overall fracture toughness.

A metallographic examination of the three mutually perpendicular directions in a wrought steel, as shown in Fig. 1, illustrate the non-uniform shape and distribution of inclusions and hence provides a qualitative explanation for the anisotropy in ductility and toughness. Events leading to such a distribution of type II MnS inclusions, the type commonly found in fully killed steels, have been considered by Baker and Charles, and their results bear repeating here (5). The inclusions

precipitate during solidification of the ingot in a "rod-shaped" morphology between dendrites. The resulting structure is referred to as interdendritic colonies of type II MnS inclusions. An example is shown in Fig. 2 as observed in a plain low carbon cast steel. The "rods" in this photograph are nearly perpendicular to the plane shown. Thus, even the original inclusion distribution is non-uniform. During subsequent hot rolling, the colonies are not only reoriented by rigid body motion so that their long dimension lies in the rolling direction in the rolling plane, but they are also plastically deformed. Regardless of whether the wrought steel is subsequently heat treated, the resulting inclusion distribution remains as shown in Fig. 1. Length, width, and thickness of inclusions are referred to as $2a_o$, $2c_o$, and $2b_o$, respectively. The prior austenite grain size is indicated at the top of Fig. 1.

Since the inclusion distribution and dimensions are so radically different in the three mutually perpendicular directions, it is natural to expect that fracture surfaces from the three fracture plane orientations, as shown in Fig. 3, will look different. Although different in appearance, all fractures <u>are microscopically ductile</u> (i.e., fracture by microvoid coalescence).

In this report, fracture surfaces from the three mutually perpendicular directions in a wrought steel plate are examined concurrently with microstructure in an attempt to better understand void growth and anisotropy in fracture properties resulting from the shape and non-uniform distribution of inclusions. First, the microscopic aspects of void growth and coalescence in martensitic steel (ductile fracture) are discussed in general, then a description is given of ductile fracture in a wrought steel for the three mutually perpendicular fracture plane orientations. From such observations, the inclusion distribution can be mathematically characterized and the anisotropy in fracture properties quantitatively appreciated. In many of the micrographs, the corresponding prior austenite grain size is illustrated for a better appreciation of relative size of fracture features with respect to important microstructural features. The chemistry and mechanical properties of the steel examined are given in Table 1.

BASIC ASPECTS OF MICROSCOPIC DUCTILE FRACTURE

A qualitative description of ductile fracture has already been provided by Cox and Low who studied plastic fracture (fracture under local plastic strain) in AISI 4340 and 18 Ni maraging steel (6). In AISI 4340 the process of plastic fracture was found to consist of void growth from inclusions first followed by void growth from Fe_3C strengthening precipitates. Voids which form from strengthening precipitates in the highly constrained region between inclusion nucleated voids are believed to occur in sheets (hence, the void sheet concept). In maraging steel the inclusion nucleated voids were found to grow until coalescence without being interrupted by void growth from strengthening precipitates. The strengthening precipitates in maraging steel, believed to be Ni_3Mo, are several orders of magnitude smaller than the non-metallic inclusions (7) and do not initiate voids until they become much larger in size from, for instance, overaging (8). This basic difference in the microscopic aspect of fracture is compatible with the observed higher fracture toughness of 18 Ni maraging steel compared to AISI 4340 when both are heat treated to the same yield strength level (6).

Figure 4 illustrates the fracture process for the two steels just described and attempts to schematically illustrate how macroscopic fracture strain is influenced by the size and number of second phase particles lying in the impending plane. Shown in Fig. 4c is an additional situation where inclusion and strengthening precipitate size are nearly equal. All transgranular ductile fracture processes in martensitic steel can be schematically described by one of these illustrations. Note in Fig. 4 that the second phase particle size which can initiate voids is smallest for the largest macroscopic fracture strain. Such a strain dependent "size effect" for void initiation from second phase particles was demonstrated experimentally by Cox and Low (6).

In ultra pure metals, reduction of areas of near 100% are possible as measured in the uniaxial tensile test. Second phase particles are absent in such metals

and other heterogeneities, submicroscopic in size (i.e., dislocation pileups or tangles, vacancy clusters, etc.,) must initiate voids. Because of their small size, unusually large plastic strains are required.

It should be emphasized that although nearly all voids in practical engineering metals are nucleated by second phase particles, all second phase particles do not initiate voids. An illustration of this was the strain dependent "size effect." Another illustration, mentioned by Russ (9), concerns the "constraint relieving effect" on near neighbor second phase particles when a void forms and grows. For instance, consider that neighbor particles have equal probability of initiating a void. One will initiate a void first and, subsequently, cause a reduction of constraint on neighboring particles which, thereafter, may never initiate a void. Figure 5 compares the number of voids on the fracture to microstructural features. The number of voids and number of prior austenite grains per unit area are nearly the same order of magnitude. Thus, only a few of the largest Fe_3C precipitates initiate voids whereas many hundreds exist per prior austenite grain (the order of 2000 to 5000).

DUCTILE FRACTURE IN WROUGHT STEEL PLATE

With only minor modifications, the principles of microscopically ductile fracture just discussed can be used to describe fracture in wrought steels which have inclusions that are anisotropic in shape and non-uniformly distributed.

WR Fracture Plane Orientation

Figure 6 illustrates the inclusion orientation from which to consider void growth for the WR fracture plane orientation. Upon load application, crystallographic slip eminates from the inclusion at some value of local stress, σ_s, which depends on the orientation of the slip plane with respect to loading direction (i.e., according to the critical resolved shear stress concept). It is possible, of course, for grains away from the inclusions to slip first if they are more favorably oriented. Subsequent loading produces slip in grains between neighboring inclusions which ultimately results in a shear band. After inclusion-nucleated void growth commences, whether it be matrix-inclusion interface separation or inclusion fracture, strain is intensified in the shear band and, additionally, its width may be increased. Finally, small voids are initiated in the shear bands at the large Fe_3C particles which themselves grow, coalesce, and produce macroscopic fracture (i.e., void sheet concept (1)). Experimental evidence of these events are present on ductile fracture surfaces as large inclusion-nucleated voids separated by smaller Fe_3C nucleated voids.

The WR fracture plane profile of Figure 7(a) demonstrates the irregularity of the fracture surface which results from void sheets connecting the large inclusion nucleated voids. Figure 7(b) shows some detail of void growth from inclusions below the actual fracture surface. Void growth occurs perpendicular to as well as in the macroscopic direction of loading. Figure 8 compares inclusions seen metallographically to inclusion-nucleated voids at the fatigue-fast fracture boundary. The

stereo fractographs clearly illustrate that, because of inclusion orientation, long cylindrically-shaped voids initiate and grow from the inclusions and that a large amount of void growth occurs transverse to the loading direction. The small voids between the large inclusion-nucleated voids form the Fe_3C nucleated void sheet referred to in Fig. 6.

RW Fracture Plane Orientation

The principles of inclusion nucleated void growth referred to in Fig. 6 apply, in general, to all fracture plane orientations. However, each orientation commands some uniqueness. In the case of the RW fracture plane orientation, the uniqueness appears only after both metallographic and fracture surface examination. Figure 9(a) shows the RW fracture plane in profile on which are displayed large voids that intersect the fracture surface. Figure 9(b) is a highly magnified view of inclusions near the fracture surface and illustrates inclusion nucleated void formation and local coalescence. A stereo view of the RW fracture plane, Fig. 10, illustrates that inclusion nucleated voids grew and coalesced in the W direction with near neighbor inclusion nucleated voids creating an elongated void. Then, final fracture occurred when the strain between the elongated voids was sufficient to initiate and grow voids from the largest cementite (Fe_3C) precipitates. The presence of shear planes between elongated voids indicates that matrix slip at $\simeq 45^\circ$ to the T direction was primarily responsible for final fracture. Note for this fracture plane orientation that inclusion nucleated void growth occurred in both directions which are perpendicular to the loading direction.

TR Fracture Plane Orientation

The TR fracture plane orientation suffers most from the shape and non-uniform distribution of inclusions. The TR fracture plane profile of Fig. 11(a) illustrates that inclusion groupings at differing elevations are joined giving a fracture surface described as a series of "plateaus." Horizontal groupings of inclusions and inclusion

nucleated voids, shown in Fig. 11(b), perhaps better illustrate how a "plateau" is formed. Unlike the WR and RW fracture plane orientations, the inclusions for the TR fracture plane orientation are often grouped close enough that inclusion nucleated voids approach coalescence before strain between them is high enough to cause cementite (Fe_3C) nucleated voids to form. The apparent "flatness" of the fracture surface is a reflection of inclusion grouping and is small in extent. The TR fracture plane orientation is shown in stereo in Fig. 12 with the proper plate orientations marked. Figure 12(a) shows the original inclusion size and shape, and the close proximity of neighboring inclusions. Lower magnification photographs indicate the generality of inclusion size and distribution. Illustrated in these photographs is the extent of void growth from inclusions. The high magnification fracture plane profile in Fig. 11(c) illustrates that in some cases (small inclusion spacing) inclusion nucleated voids coalesced directly, whereas for larger inclusion spacings a small Fe_3C nucleated void sheet formed linking the inclusion nucleated voids.

DISCUSSION

From the foregoing descriptions of fracture for the three mutually perpendicular fracture plane orientations, it becomes possible to describe a model which characterizes the inclusion distribution in wrought steel. A schematic illustration of the inclusion distribution is shown in Fig. 13 which is a likeness of either Figs. 1 or 3. Figures 7, 9, and 11 illustrated the fracture path for the WR, RW, and TR fracture plane orientations. From these figures it was possible to appreciate why, for instance, fracture strain for the WR orientation was much higher than for the TR orientation. Fracture strain has been shown to be a function of volume fraction of second phase particles, V_v (3). Considering fracture path, it is easily seen that the effective volume fraction for the WR orientation is much less than for the TR orientation. In fact, calculations can show that the effective volume fraction for the TR fracture plane orientation is several times larger than that when the inclusions are randomly distributed.

Consider that the inclusion distribution can be described as inclusion groupings of size, ℓ_{ij}, spaced a distance, p, apart on planes of average spacing, s. The area, shown in Fig. 13, can be separated into sub-areas of size s by L, the transverse length across the fracture. For each s by L area the inclusions occupy an area ℓ_{ij} by s with an area 1 - ℓ_{ij} s free of inclusions. Since fracture for the TR fracture plane orientation follows the ℓ_{ij} by s areas giving the "plateaus" on the fracture surface, the effective volume fraction of inclusions is very large. The volume fraction for random inclusion distribution, V_v, is:

$$\frac{\text{Vol. inclusions}}{\text{Vol. material}} = \frac{\overline{N}\,\pi\, c_o\, b_o}{Ls} = V_v \qquad (1)$$

$\overline{N}$ = average number of inclusions per length L

The effective volume fraction of inclusions for the TR fracture plane orientation, V_v', is

$$\frac{\text{Vol. inclusions}}{\text{Vol. fracture path}} = \frac{(N_{31} + N_{21} + N_{41} + N_{32} + N_{51})\,\pi\, c_o\, b_o}{LS}$$

$$= \left(\frac{\overline{n_{ij}}}{\ell_{ij}}\right) \frac{\pi\, c_o\, b_o}{S} = V_v' \qquad (2)$$

where $S = Hs$ = average "step distance" between plateaus perpendicular to macroscopic fracture plane (see Fig. 13)

$\left(\frac{\overline{n_{ij}}}{\ell_{ij}}\right)$ = average center-to-center spacing of inclusions in grouping

The ratio V_v'/V_v is

$$\frac{\left(\frac{\overline{n_{ij}}}{\ell_{ij}}\right)}{\left(\frac{\overline{NH}}{L}\right)} = \frac{V_v'}{V_v} \qquad (3)$$

and by moving the average sign inside parenthesis, one can show that the ratio is

$$\frac{HV_v'}{V_v} \geq \frac{L}{\left(\frac{\overline{N}}{\overline{n_{ij}}}\right)} \frac{1}{\ell_{ij}} = \frac{p}{\ell_{ij}} \qquad (4)$$

which is the periodicity or spacing of inclusion groupings divided by the average size of inclusion groups. Both quantities can be determined by fracture plane profile examination. Table 2 gives the results of such examination for the TR fracture profile. The periodicity of inclusion groupings, p, was obtained from the average number of ℓ_{ij} groups at each index position (see Fig. 13). The $\overline{\ell}_{ij}$ was found from the number of ℓ_{ij} units per unit distance across the fracture. Two hardness levels for a given steel were examined and the ratio HV_v'/V_v was found to be 25 for both. The value

of H was determined by averaging the "step distance" between plateaus, as illustrated in Fig. 13 and Table 2. The average "step distance" for the lowest hardness steel was greater than that for the high hardness. Such an observation is compatible with the low hardness steel being less "inclusion sensitive" than the higher hardness steel. Thus, in calculating fracture strain from its proposed functional relationship to volume fraction second phase particles, Eq. 5, it is necessary to use the effective volume fraction rather than the actual volume fraction base on random distribution of inclusions.

$$\epsilon_f = k \left(\frac{1 - V_v}{V_v} \right) \tag{5}$$

V_v = effective volume fraction second phase particles

Without detailed knowledge on the extent of local plastic strains above and below the RW and WR fracture planes, it is impossible to determine any difference in V_v for these fracture plane orientations. Thus, a ratio of RW to WR fracture strain would give unity. Strain concentration effects associated with inclusion shape would probably increase the ratio to values between 1 and 2 (strain concentration factor of up to 2). In high strength wrought steels the RW true fracture strain is normally between 1 and 2 times the WR true fracture strain. Comparison of fracture strains for the RW and TR fracture plane orientations, considering only effective volume fraction of inclusions, gives a ratio (RW to TR) of at least 4 as indicated in Table 2. Recognizing again that strain concentration effects of inclusion shape can contribute a factor of between 1 and 2, it is seen that the TR fracture strain is of the order of 10% of the RW fracture strain. Such values have been observed with respect to true fracture strain obtained in the uniaxial tensile test (10).

A more complete understanding of the effect of inclusion shape anisotropy on fracture strain must await a detailed mathematical analysis of multiaxial void growth

in a non-continuum. Multiaxial growth of voids from inclusions was illustrated in Figs. 7 through 12. Figure 1 showed that each inclusion was surrounded by a non-continuum, the prior austenite grain, of about 10^{-3} inches in extent (ASTM grain size 7-8) which is larger than the b_o and c_o dimensions of the largest inclusions.

The fractographic results of this investigation further illustrate that improvements in ductility and toughness at high strength levels will result from fewer and less severely deformed inclusions. Naturally, fewer inclusions imply improvements in steel-making practice (i.e., vacuum treatments such as vacuum induction melting, etc.). It has been known for some time that the amount of inclusion deformation depends on rolling temperature (5, 11), but the application of such knowledge has only recently been commercially available. Also, the addition of rare earth metal to the ladle gives rare earth sulfides, which are more difficult to deform upon rolling than the conventional type II manganese sulfides. Thus, certain of the obvious methods of increasing toughness are now available.

CONCLUSIONS

Fracture surface examination of the three mutually perpendicular fracture plane orientations resulted in the following observations which supplement existing information on microscopic aspects of fracture.

1. Void growth from inclusions occurred transverse to the loading direction. The extent of transverse void growth depended on fracture plane orientation, but was observed to be as much as ten times the b_o dimension (i.e., smallest dimension) of the inclusion.
2. Of the hundreds of strengthening precipitates present per prior austenite grain, only a few participated in void nucleation and growth during fracture.
3. The non-uniform distribution of inclusions and the anisotropy in their shape were responsible for the differences in fractographic features on the three mutually perpendicular fracture plane orientations.
4. The mathematical characterization of inclusion distribution illustrated that effective volume fraction of inclusions depended on fracture plane orientation and, hence, aided in the understanding of anisotropy in fracture strain.

The intent of this assemblage of information is to describe, at least qualitatively, the ductile fracture process as it occurs in conventional wrought martensitic steels. The photographic data was collected by both optical and scanning electron microscopy. Fracture profile analysis and metallography was as important to the interpretation of the fracture process as was fracture surface analysis. The low magnifications used serve to make the interpretation general in nature.

REFERENCES

1. H. C. Rogers, "Effect of Material Variables on Ductility," Ductility, American Society for Metals, Metals Park, Ohio, 1968, Chapter 2.

2. A. J. Birkle, R. P. Wei, and G. E. Pellissier, "Analysis of Plane Strain Fracture in a Series of 0.45 C-Ni-Cr-Mo Steels with Different Sulfur Contents," Trans. Quarterly ASM, Vol. 59, 1966, p. 981.

3. J. J. Hauser and M. G. H. Welk, "Inclusions in High Strength Steels--Their Dependence on Processing Variables and Their Effect on Engineering Properties," Tech. Report AFML-TR-68-222, August, 1968.

4. B. I. Edelson and W. M. Baldwin, Jr., "The Effect of Second Phases on the Mechanical Properties of Alloys," Trans. Quarterly ASM, Vol. 55, 1962, p. 230.

5. T. J. Baker and J. A. Charles, "Type II Manganese Sulphides: Their Deformation and Effect on Steel Fracture," JISI, Vol. 211, 1973, p. 187.

6. T. B. Cox and J. R. Low, Jr., "An Investigation of the Plastic Fracture of High Strength Steels," NASA Tech. Report No. 3, Dept. of Metallurgy and Materials Science, Carnegie-Mellon University, May, 1972.

7. S. Floreen, "The Physical Metallurgy of Maraging Steel," Metallurgical Reviews, Review No. 126, 1968, p. 115.

8. L. Roesch and G. Henry, "Relationship between Precipitation and Dimple Fracture in an 18 Percent Nickel Maraging Steel," Electron Microfractography, ASTM STP 453, Philadelphia, Pennsylvania, 1969.

9. J. C. Russ, ibid, discussion to Ref. 8.

10. J. C. M. Farrar, J. A. Charles, and R. E. Dolby, "Metallurgical Aspects of Lamellar Tearing," ISI Spec. Pub. #145, 1971, p. 79.

11. T. Malkiewicz and S. Rudnik, "Deformation and Non-metallic Inclusions during Rolling of Steel," JISI, Vol. 202, 1963, p. 33.

TABLE 1

CHEMISTRY AND MECHANICAL PROPERTIES OF STEEL INVESTIGATED*

C	Mn	P	S	Si	Cr	Mo	Al	B
0.17	1.06	0.009	0.019	0.23	0.40	0.29	0.02	0.0006

Ultimate Strength		Yield Strength		R. A.	WR Fracture Toughness	
ksi	(N/mm^2)	ksi	(N/mm^2)	%	ksi $\sqrt{in}$	($N_{mm}^{3}/2$)
171	(1170)	161	(1100)	42	73 $\pm$ 2	(2510 $\pm$ 70)

*Steel underwent conventional hot rolling, then was quenched and tempered.

TABLE 2

SUMMARY OF STATISTICAL MEASUREMENTS
FOR SHORT TRANSVERSE FRACTURE PLANE PROFILE

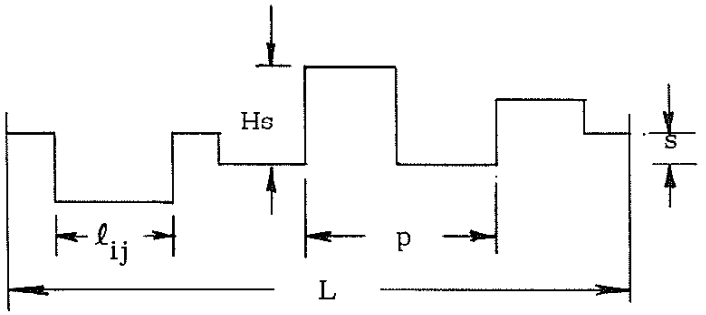

Hardness, R_c	$\bar{p}$ in	$\bar{p}$ (mm)	$\bar{\ell}_{ij}$ in	$\bar{\ell}_{ij}$ (mm)	$\frac{\bar{p}}{\bar{\ell}_{ij}}$	$\bar{H}$	$\frac{V_v'}{\bar{V}_v}$
35	0.19	(4.8)	0.0076	(0.192)	25	5.7	4.4
25	0.13	(3.3)	0.0053	(0.134)	25	6.4	3.9

Note: Bars over symbols denote average values.

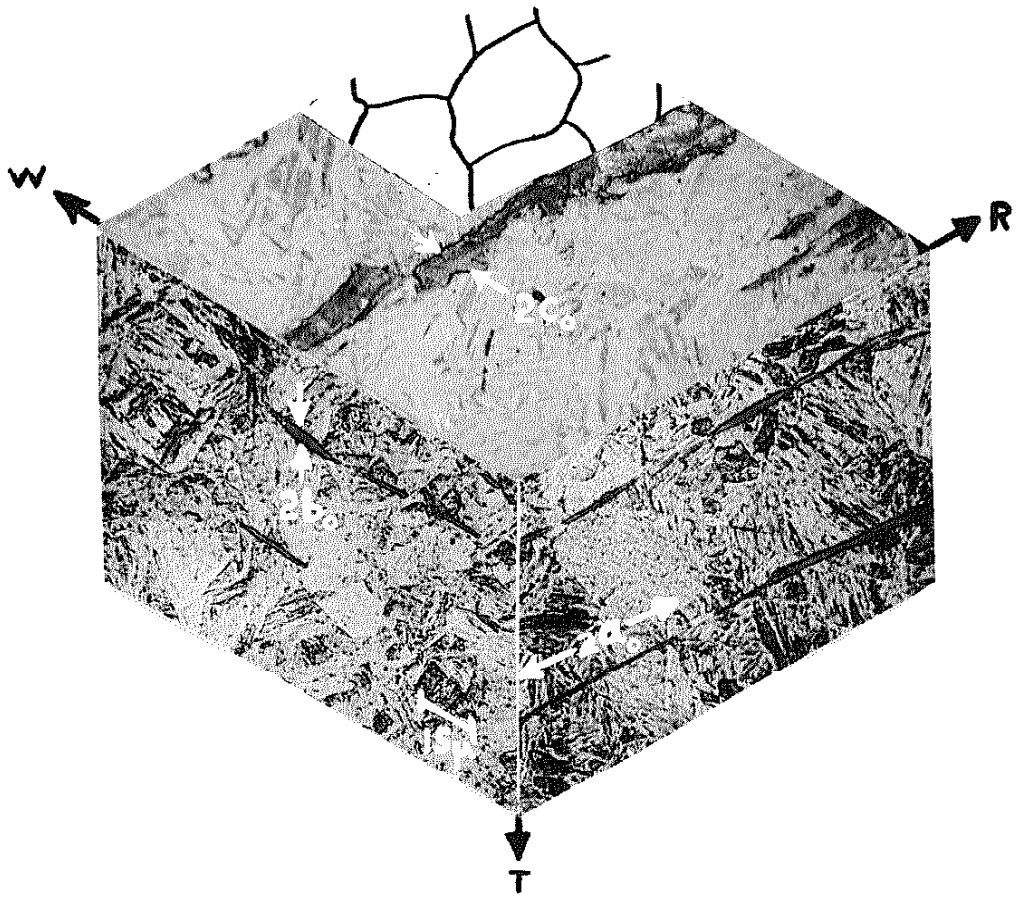

FIG. 1 ISOMETRIC PRESENTATION OF INCLUSIONS IN WROUGHT STEEL (MAG. 750X)

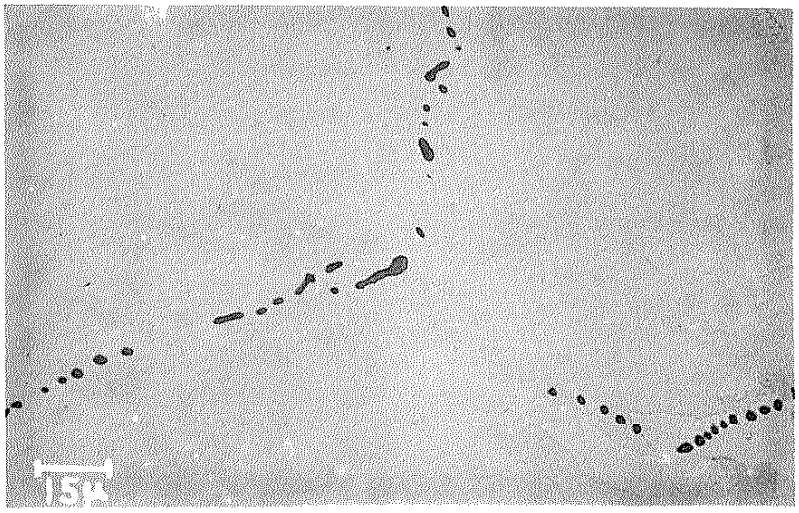

FIG. 2 INTERDENDRITIC COLONIES OF TYPE II MnS INCLUSIONS IN CAST STEEL (MAG. 750X)

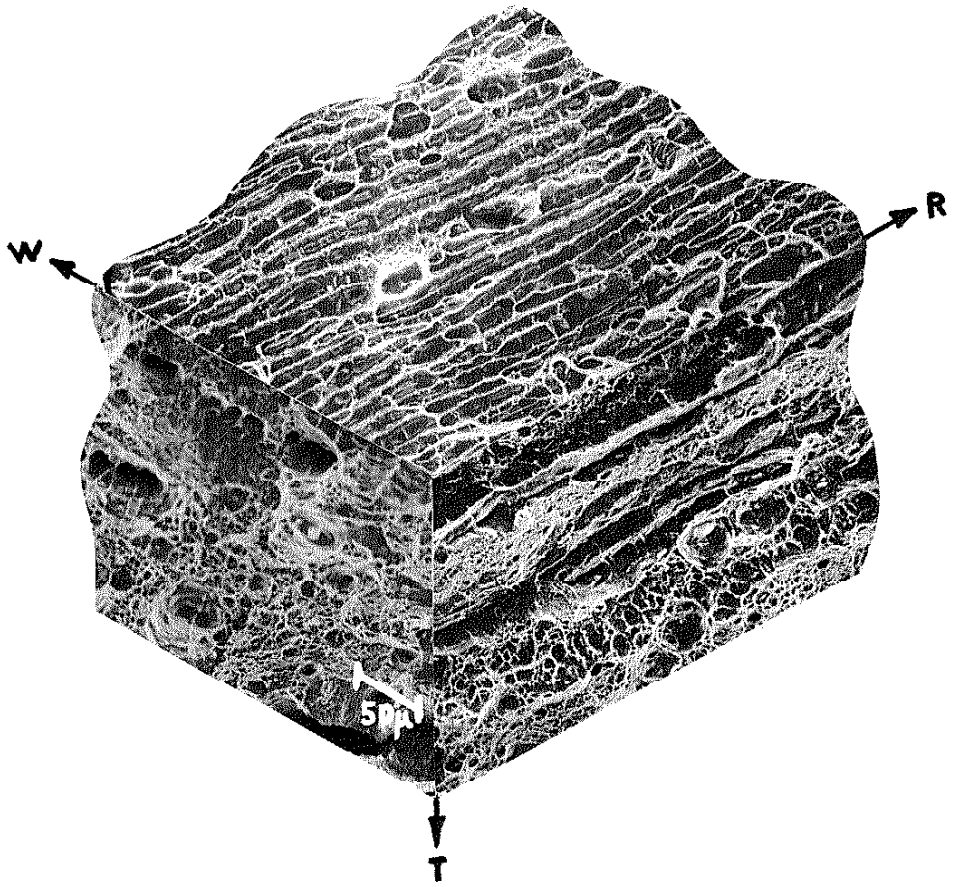

FIG. 3 ISOMETRIC PRESENTATION OF FRACTURE FEATURES FROM MUTUALLY PERPENDICULAR DIRECTIONS IN WROUGHT STEEL. ALTHOUGH DIFFERENT IN APPEARANCE, ALL FRACTURES ARE MICROSCOPICALLY DUCTILE (MAG. 200X)

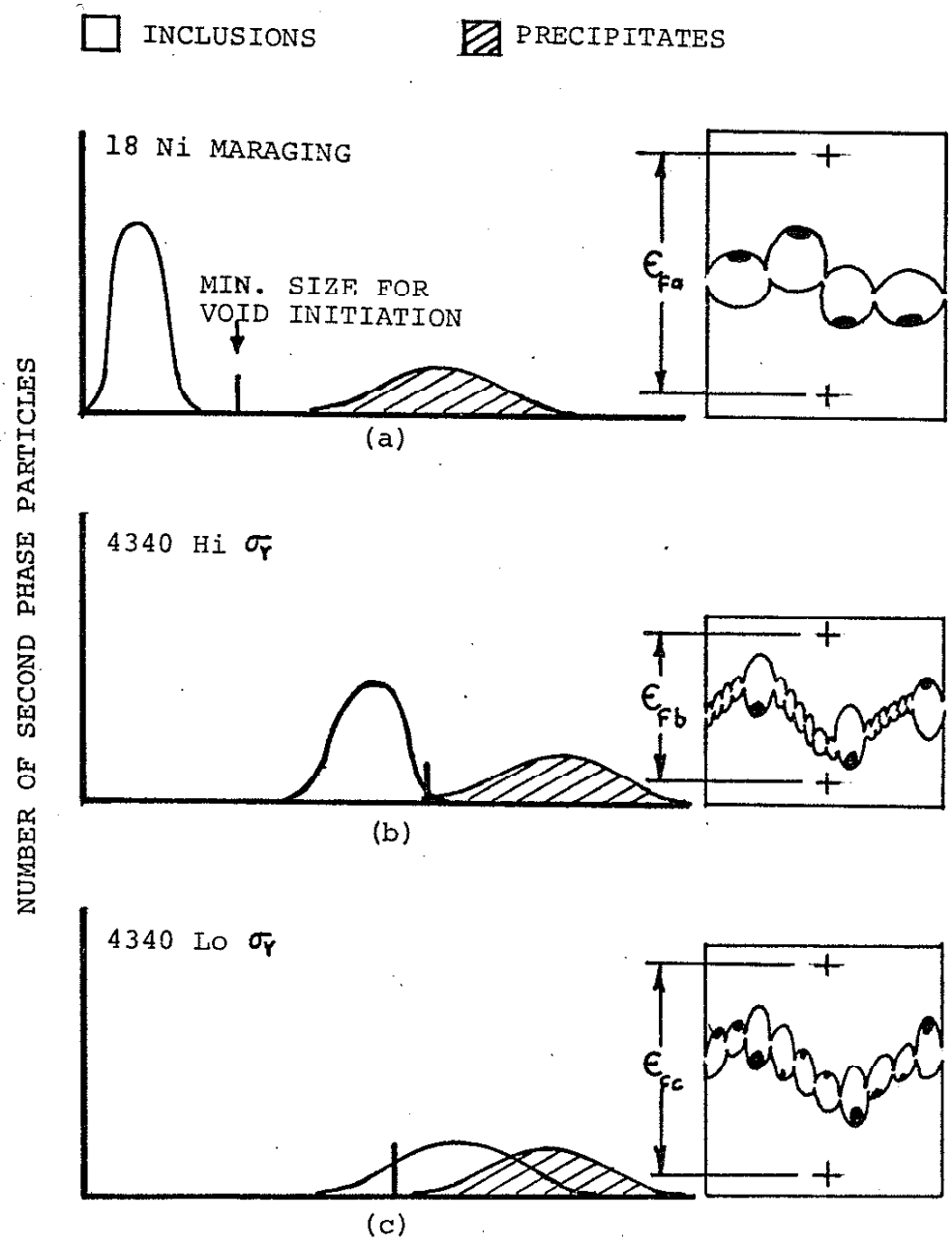

FIG. 4 SCHEMATIC ILLUSTRATION INDICATING HOW SIZE OF INCLUSIONS AND STRENGTHENING PRECIPITATES AFFECT VOID INITIATION, GROWTH, AND SUBSEQUENT FRACTURE STRAIN IN MARTENSITIC STEELS

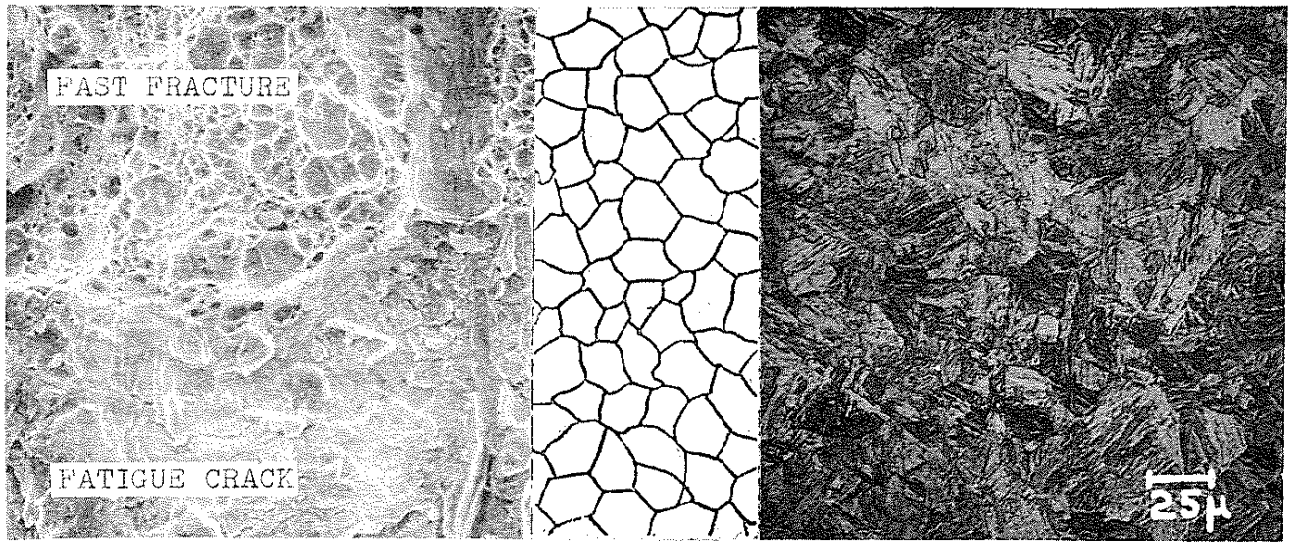

FIG. 5 COMPARISON OF MICROSTRUCTURAL FEATURES AND FRACTURE SURFACE FEATURES IN A HSLA WROUGHT STEEL (σ_f = 160 ksi, MAG. 400X)

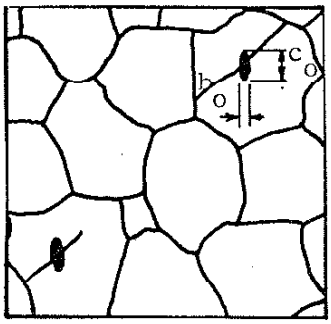

(a) LOCAL STRESS σ_s REACHED, PERMITS CRYSTALLOGRAPHIC SLIP TO OCCUR NEAR INCLUSION

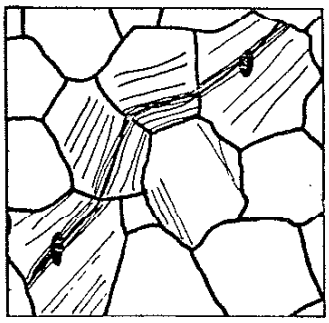

(b) FURTHER LOADING CAUSES SLIP IN ALL GRAINS BETWEEN INCLUSIONS

LOADING DIRECTION

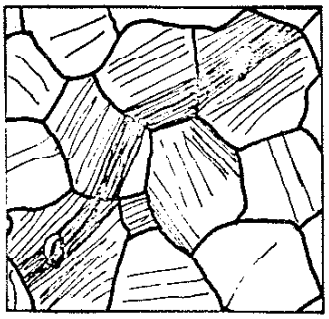

(c) MATRIX-INCLUSION INTERFACE SEPARATION OCCURS, STRAIN IS INTENSIFIED IN SLIP BAND, SLIP BAND WIDTH INCREASES

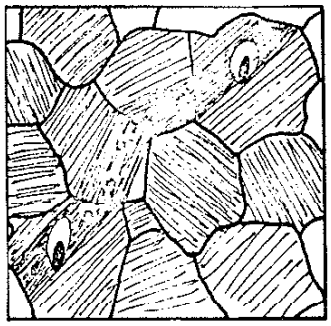

(d) CEMENTITE INITIATED VOIDS FORM IN SHEAR BAND, GROW, EVENTUALLY FORM A VOID SHEET BETWEEN INCLUSIONS PRODUCING MACRO FRACTURE.

FIG. 6 SCHEMATIC ILLUSTRATION OF SHEAR BAND FORMATION AND VOID GROWTH FROM INCLUSIONS FOR THE WR FRACTURE PLANE ORIENTATION. (ROLLING DIRECTION NORMAL TO PLANE OF FIGURES)

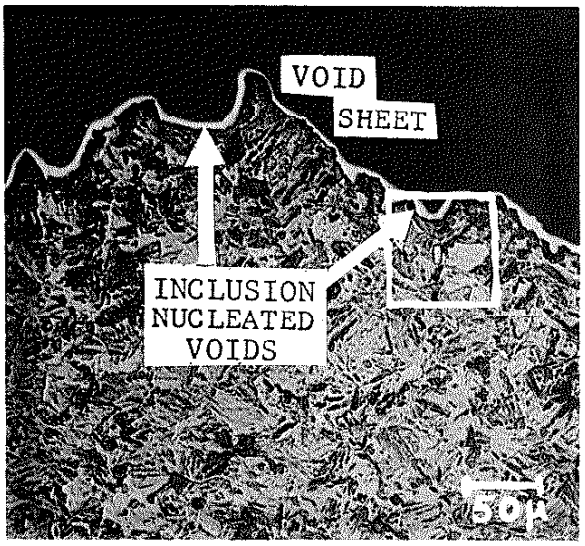

(a) MAG. 200X

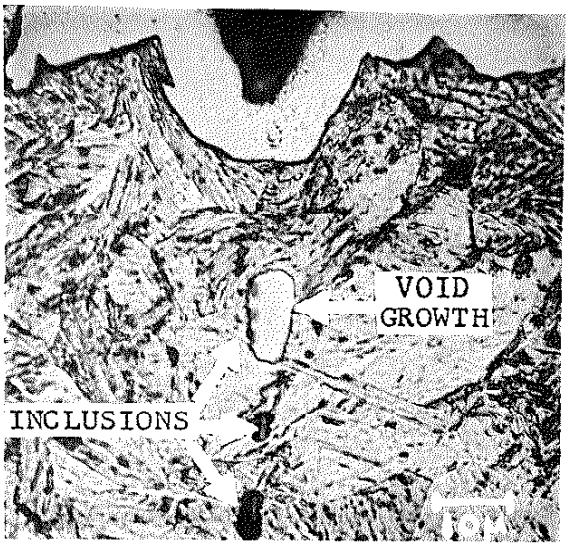

(b) MAG. 1000X

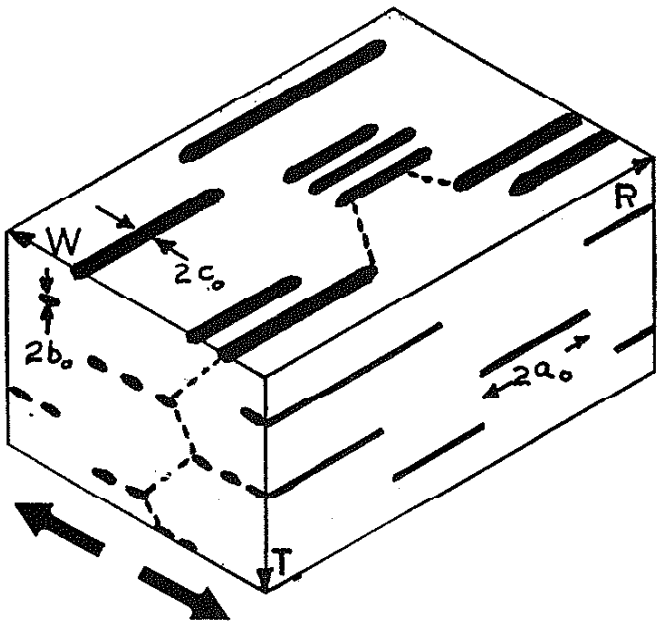

FIG. 7 WR FRACTURE PLANE ORIENTATION (a) Ni PLATED FRACTURE PLANE PROFILE, (b) DETAILS OF VOID FORMATION AND GROWTH FROM INCLUSIONS. ILLUSTRATION SHOWS LOADING DIRECTION WITH RESPECT TO INCLUSION SIZE AND DISTRIBUTION, AND SUBSEQUENT FRACTURE PATH.

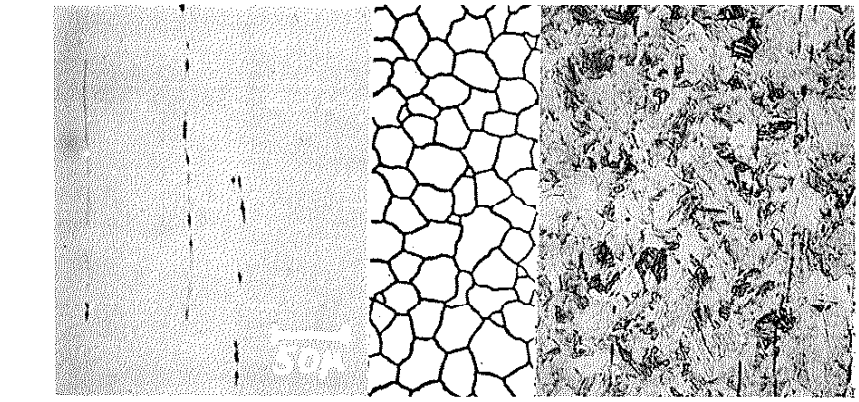

(a)

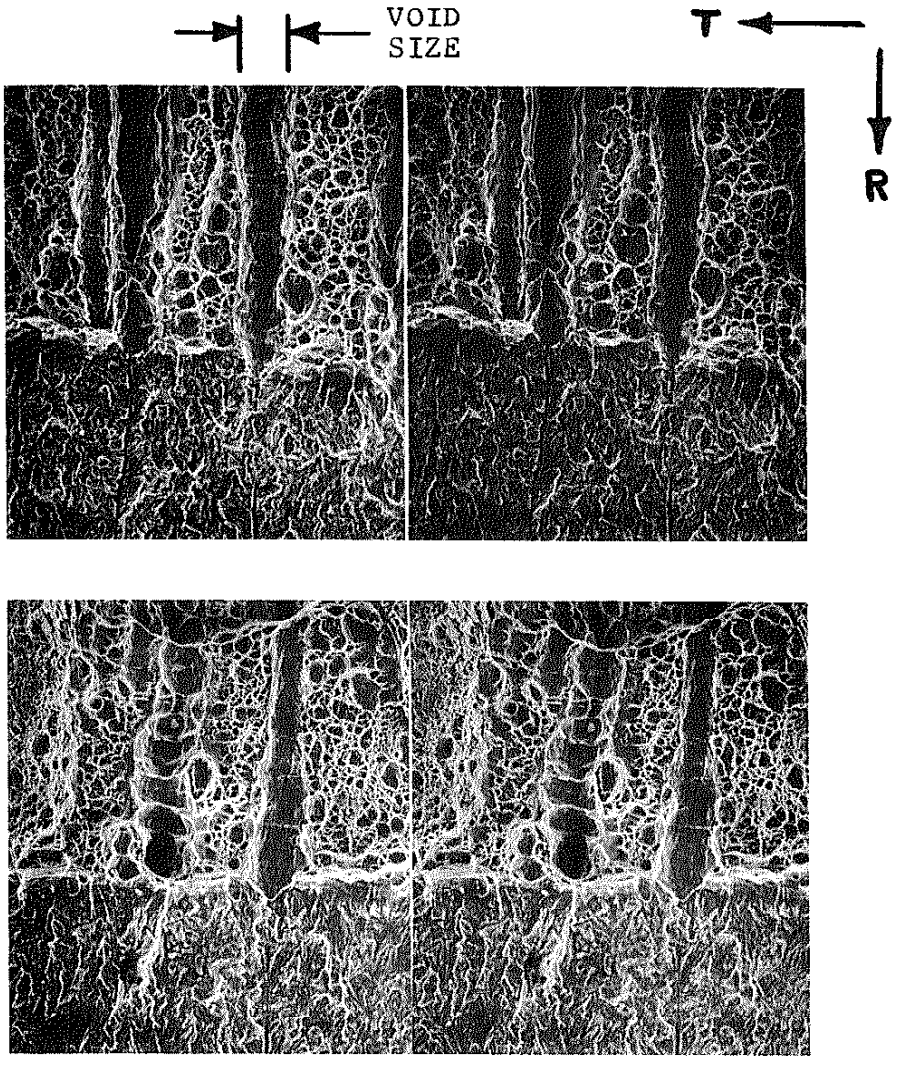

(b)

FIG. 8 (a) MICROSTRUCTURAL FEATURES OF WROUGHT STEEL
(b) STEREO FRACTOGRAPHS ILLUSTRATING INCLUSION NUCLEATED VOID GROWTH TRANSVERSE TO LOADING DIRECTION. (ALL MAG. 200X)

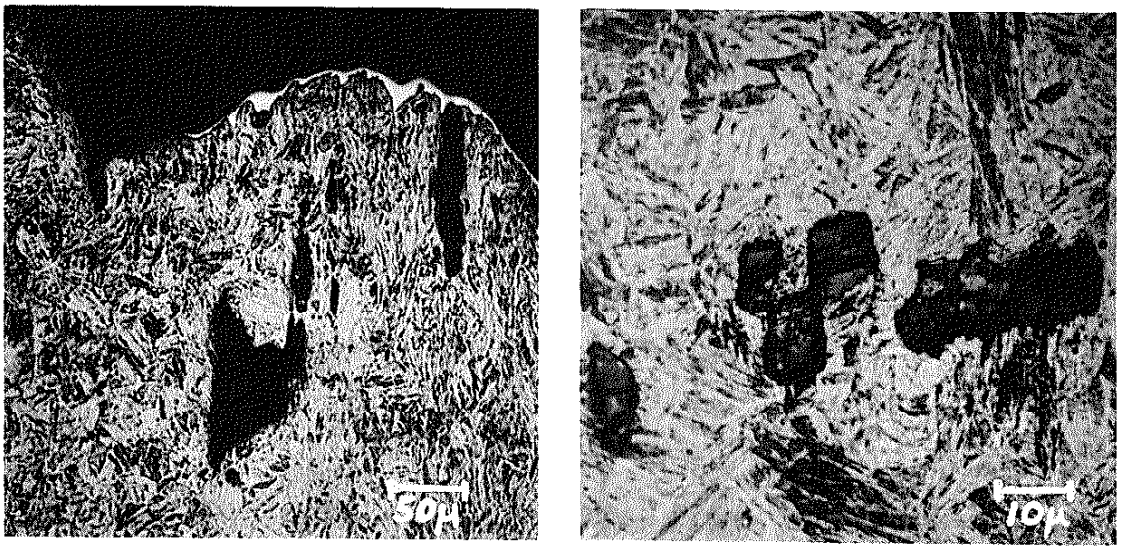

(a) MAG. 200X (b) MAG. 1000X

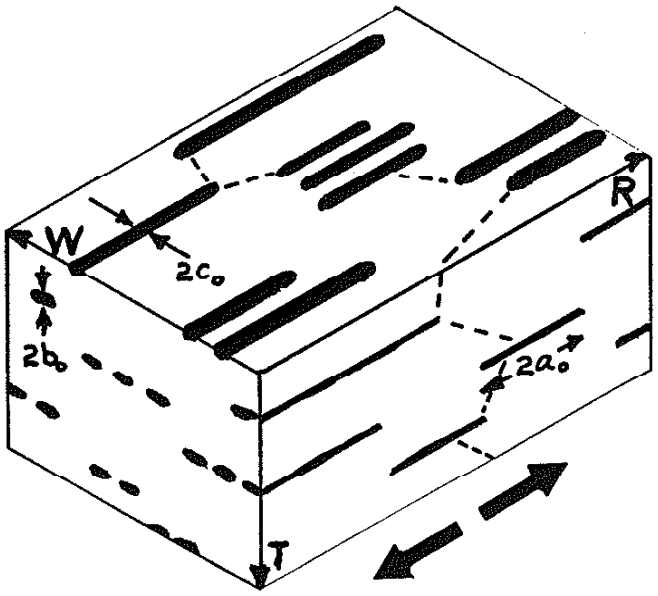

FIG. 9 RW FRACTURE PLANE ORIENTATION (a) Ni PLATED FRACTURE PLANE PROFILE SHOWING INCLUSION NUCLEATED VOIDS. (b) DETAILS OF VOID FORMATION AND COALESCENCE. ILLUSTRATION SHOWS LOADING DIRECTION WITH RESPECT TO INCLUSION SIZE AND DISTRIBUTION, AND SUBSEQUENT FRACTURE PATH.

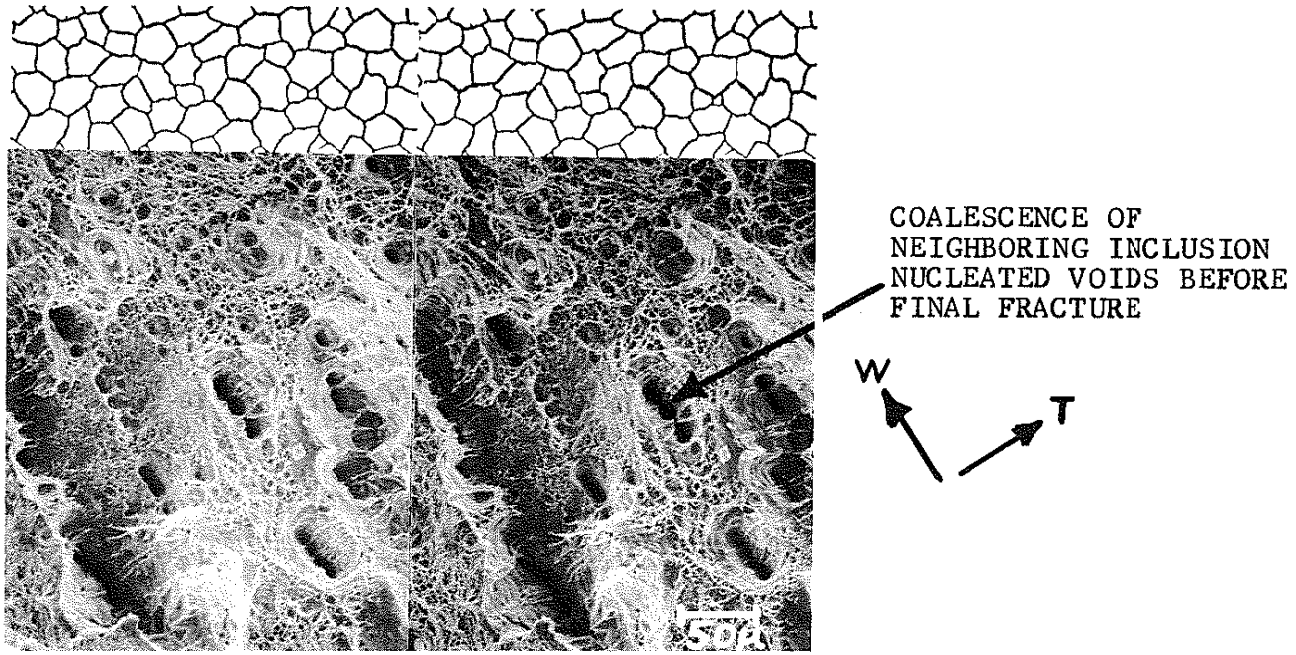

FIG. 10 STEREO FRACTOGRAPH OF RW FRACTURE PLANE ORIENTATION. PRIOR AUSTENITE GRAIN SIZE INDICATED (MAG. 200X)

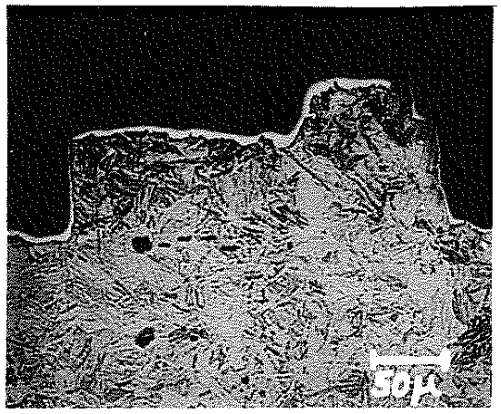

(a) MAG. 200X

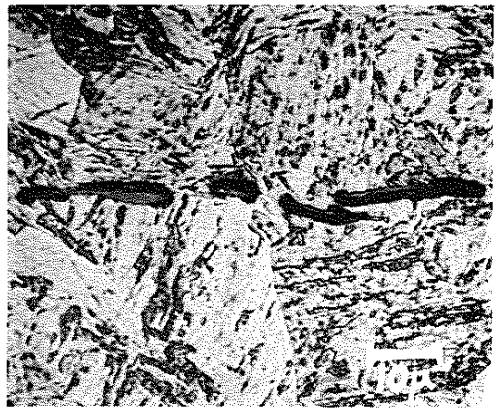

(b) MAG. 1000X

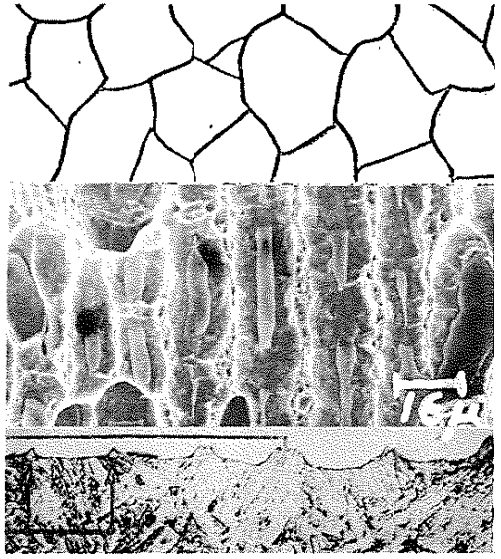

(c) MAG. 600X

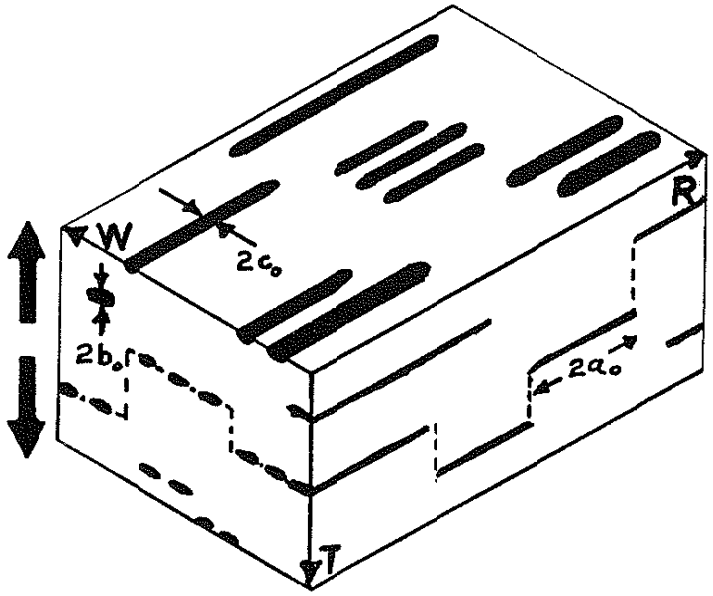

FIG. 11 TR FRACTURE PLANE ORIENTATION (a) Ni PLATED FRACTURE PLANE PROFILE (b) DETAILS OF VOID FORMATION AND GROWTH (c) FRACTOGRAPH WITH CORRESPONDING FRACTURE PLANE PROFILE. ILLUSTRATION SHOWS LOADING DIRECTION WITH RESPECT TO INCLUSION SIZE AND DISTRIBUTION, AND SUBSEQUENT FRACTURE PATH.

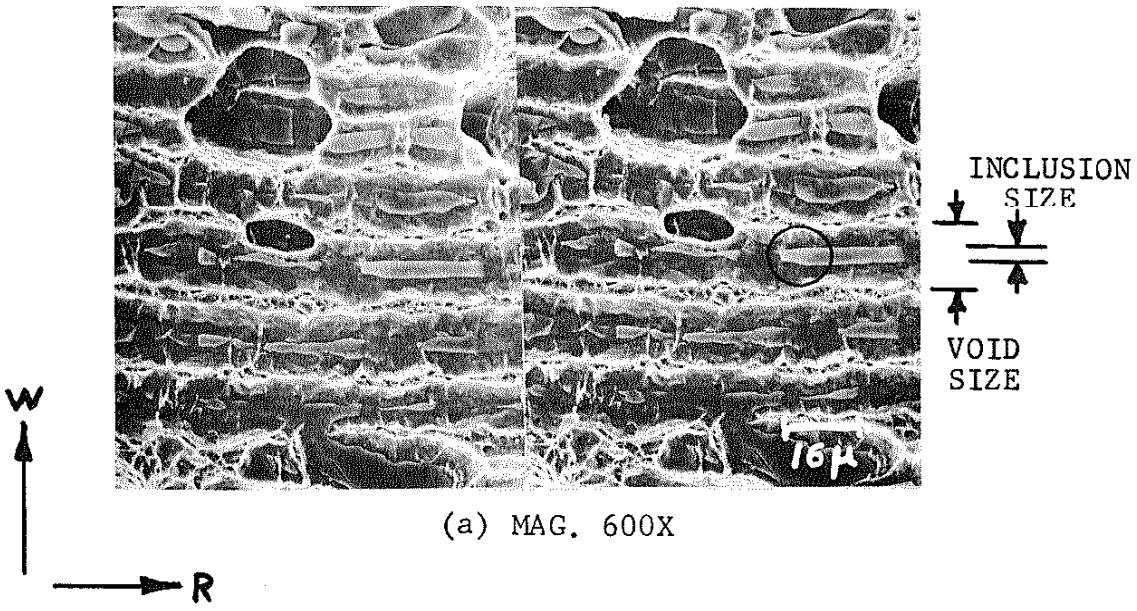

(a) MAG. 600X

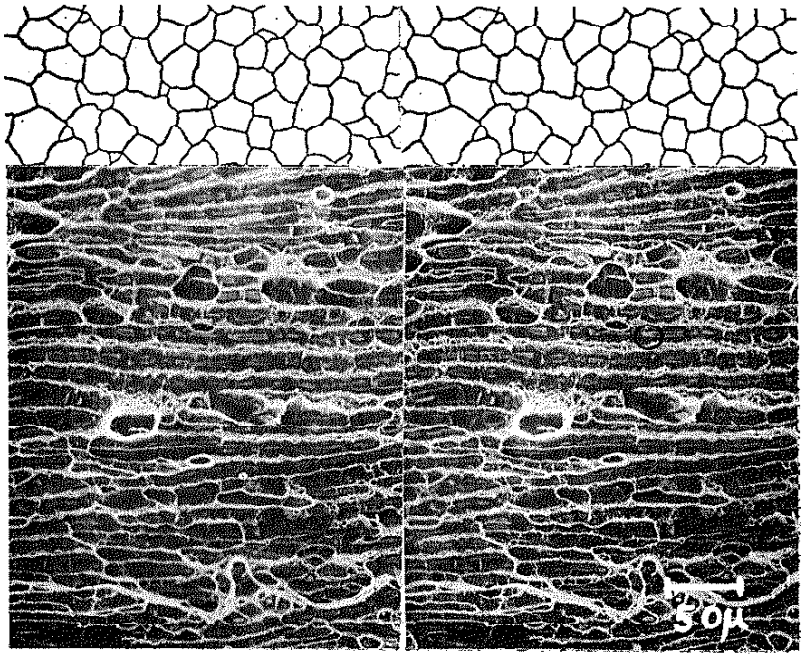

(b) MAG. 200X

FIG. 12 STEREO FRACTOGRAPHS SHOWING INCLUSIONS AND VOID GROWTH ON TR FRACTURE PLANE.

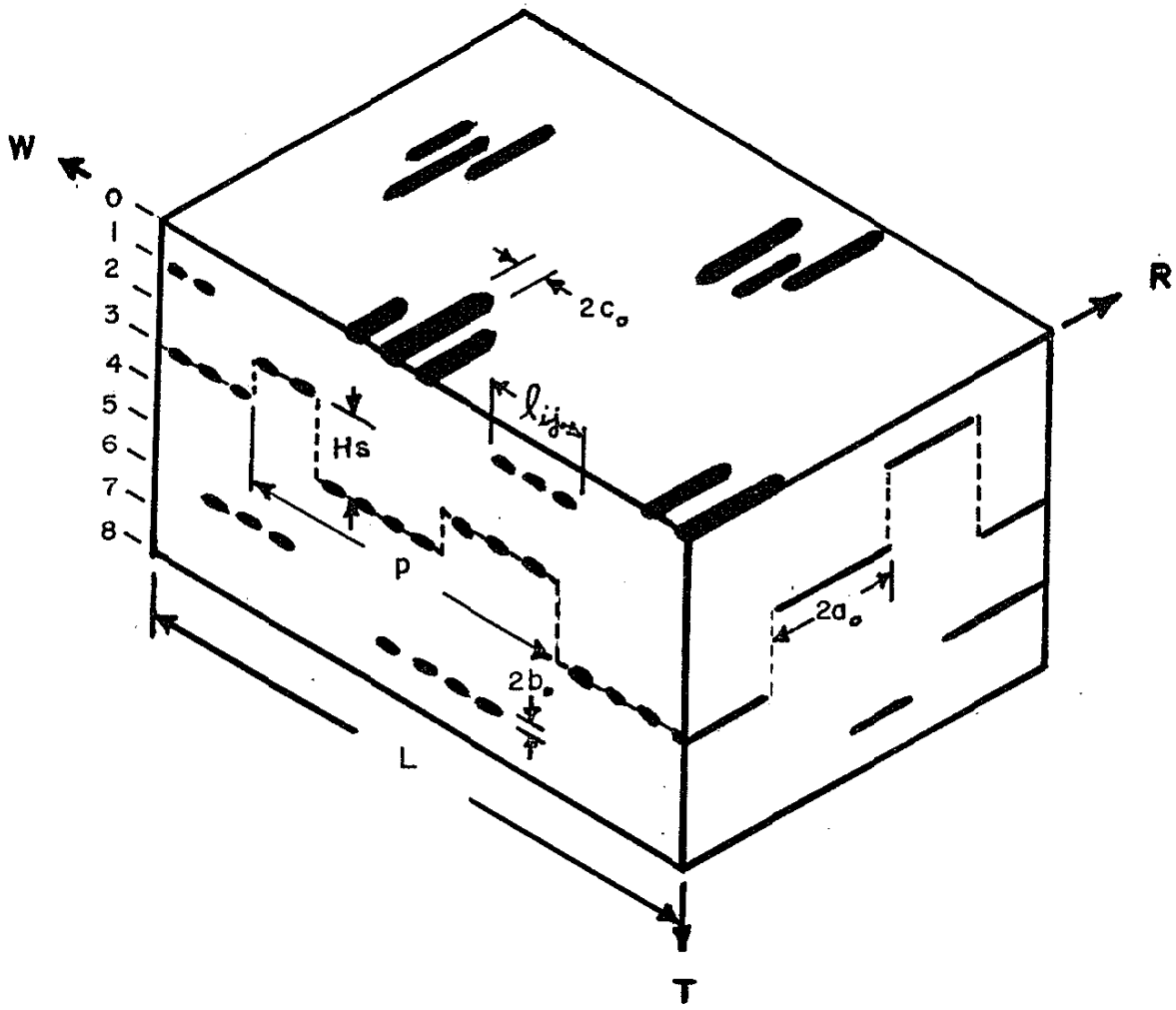

FIG. 13 SCHEMATIC ILLUSTRATION OF INCLUSION DISTRIBUTION. FRACTURE PATH SHOWN IS FOR TR OR TW FRACTURE PLANE ORIENTATION.